

Relaxation dynamics of deuterated formyl and isoformyl cations

R. Wester,^{a)} U. Hechtfisher, L. Knoll, M. Lange, J. Levin, M. Scheffel, D. Schwalm, and A. Wolf

Max-Planck-Institut für Kernphysik, Saupfercheckweg 1, 69117 Heidelberg, Germany

A. Baer, Z. Vager, and D. Zajfman

Weizmann Institute of Science, 79100 Rehovot, Israel

M. Mladenović and S. Schmatz

Institut für Physikalische Chemie, Georg-August-Universität Göttingen, Tammannstrasse 6, 37077 Göttingen, Germany

(Received 18 October 2001; accepted 28 January 2002)

Vibrational relaxation and isomerization of internally excited deuterated formyl and isoformyl cations has been investigated on the time scale of 2 ms to 12 s using the nearly interaction-free environment of an ion storage ring. De-excitation of the ν_2 bending modes of DCO^+ and DOC^+ due to spontaneous radiative transitions was observed as a function of the storage time by measuring their foil-induced Coulomb explosion using three-dimensional coincident fragment imaging. No isomerization of low-lying vibrational levels of DOC^+ ions was observed on the time scales considered. By comparing the Coulomb explosion data to molecular bond angle distributions obtained from vibrational wave function calculations, the time evolution of the mean ν_2 population is deduced for both isomers. The stored DOC^+ ions are found to thermalize with the 300 K black-body radiation, while relaxation of the DCO^+ bending vibrations was found to require considerably longer times, in agreement with a predicted very small transition moment of the $\nu_2 = 1$ level. © 2002 American Institute of Physics. [DOI: 10.1063/1.1461812]

I. INTRODUCTION

In low density gas-phase environments, such as planetary atmospheres or molecular clouds, spontaneous radiative relaxation is the dominant cooling mechanism for internally excited molecules. Since reaction rates, product distributions, and branching ratios may significantly depend on the reactants' vibrational excitation, modeling the gas-phase chemistry in such environments relies on information regarding the internal excitation of the involved molecules and their rate of change. While at typical temperatures of 10 to 100 K only the lowest vibrational levels are expected to be populated assuming equilibrium conditions, shock waves or external radiative heating, which occur in star-forming regions, may require kinetic information on relaxation rates. Furthermore, absolute radiative transition probabilities are needed when deducing molecular abundances from line strengths of infrared emission features.

For molecular ions, which dominate the chemistry at low densities, very little laboratory data are available on spontaneous radiative transitions, essentially due to the experimental difficulties to both store the molecules interaction-free and study their internal excitation during the storage. Therefore, theoretical calculations are frequently used when radiative transition probabilities are required in chemical cloud models or the analysis of infrared emission spectra. Experimentally, vibrational lifetimes for several small molecular

ions have been obtained with the monitor ion technique, including HCO^+ and the stretching modes of DCO^+ .² The lifetimes are extracted by measuring the product yield of stored molecular ions reacting with buffer gas as a function of storage time, using buffer gas reactions that are exothermic only when the molecular ions are vibrationally excited. A new possibility of measuring vibrational lifetimes of molecules has been opened up recently by combining a storage ring with a Coulomb explosion imaging setup as described below. This technique has already been successfully used to determine vibrational lifetimes of HD^+ for $\nu=0$ to 11.^{3,4}

In this work we report an investigation of the vibrational relaxation of the bending modes of DCO^+ and its isomeric variant DOC^+ . HCO^+ and DCO^+ are abundant molecular ions in the interstellar medium, HCO^+ being the first triatomic molecular ion to be astrophysically observed,⁵ and their spectra reveal substantial information, e.g., regarding the proton–deuteron isotope ratio in molecular clouds.⁶ Using infrared absorption spectroscopy, the ν_1 ⁷ and ν_3 ⁸ stretching fundamental bands were investigated for DCO^+ , whereas to our knowledge the bending fundamental band has not been detected this way, in contrast to HCO^+ , where all fundamental bands have been observed.^{9–14} The bending fundamental transition of DCO^+ has only very recently been measured using double resonance vibrational autoionization spectroscopy of high Rydberg states of DCO converging to vibrationally excited states of DCO^+ .¹⁵ The lack of infrared absorption data indicates a low transition moment for the DCO^+ bending mode, a conjecture which is supported by the only available calculation of Sebald,¹⁶ who predicts a life-

^{a)}Present address: Department of Chemistry, University of California Berkeley, Berkeley, California 94720. Electronic mail: roland@radon.cchem.berkeley.edu

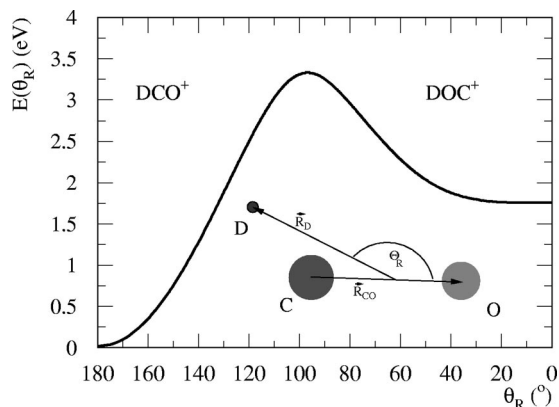


FIG. 1. Cut through the CCSD(T) potential energy surface (taken from Ref. 18) for the $\text{DCO}^+/\text{DOC}^+$ system as a function of the Jacobi angle θ_R (see the inset). The energy is minimized with respect to the two Jacobi distances for each value of the Jacobi angle.

time of 13 s for the lowest bending level of DCO^+ ; due to a strong isotope effect, this lifetime is about 40 times longer than the corresponding lifetime in HCO^+ . On the other hand, the radiative lifetimes for the lowest ν_1 and ν_3 stretching vibrational levels of DCO^+ are calculated to be 50.8 and 18.1 ms, respectively,¹⁶ i.e., much shorter as compared to that of the bending mode. The only experimental lifetime up to now has been reported by Heninger *et al.*,² who obtained a reasonable agreement for the lowest ν_3 level (24 ± 2.5 ms), but found a deviation by a factor of 4 from the calculation for the lowest ν_1 level (226 ± 45 ms), which is attributed to a vibrational coupling of the $(\nu_1, \nu_2, \nu_3) = (1, 0^1, 0)$ level to the $(0, 1^1, 1)$ level. For the first excited bending mode of DCO^+ they could only set a lower limit of about 6 s to the lifetime.

The DOC^+ isomer was first detected in a millimeter wave spectroscopy experiment in 1986.¹⁷ As can be seen from Fig. 1, which shows a cut through a recently published 3D Born–Oppenheimer potential surface for the formyl/isoformyl system,¹⁸ the DOC^+ potential minimum lies 1.7 eV above the DCO^+ minimum and the barrier height for isomerization to DCO^+ is 1.6 eV. Only for the isotopomer HOC^+ has a vibrational transition been observed, namely the ν_1 stretching fundamental band.¹⁹ The first interstellar observation of HOC^+ ²⁰ was confirmed only in 1995,²¹ pointing to an abundance ratio $[\text{HCO}^+]/[\text{HOC}^+]$ of 140–360, much smaller than expected from model calculations.²¹ Vibrational lifetime measurements or calculations for the DOC^+ isomer have not been reported to date.

The investigation of the DCO^+ and DOC^+ molecular ions presented in this paper was performed using the foil-induced Coulomb explosion imaging (CEI) technique in conjunction with the heavy ion test storage ring (TSR) at the Max-Planck-Institut für Kernphysik in Heidelberg.^{22,23} This technique allows measurement of the spatial structure distributions of molecular ion ensembles at different time delays with respect to their production in the ion source, corresponding to different degrees of internal relaxation. By comparing the measured structure distributions with theoretical distributions deduced from calculated vibrational wave func-

tions, the relative population of excited vibrational states can be monitored. With this technique, e.g., the vibrational lifetimes in HD^+ have been measured⁴ and the rate coefficient for dissociative recombination of HD^+ could be determined as a function of its vibrational excitation.³ Moreover, vibrational de-excitation rates of H_2^+ due to superelastic collisions with free electrons could be studied.²⁴ The experiment on DCO^+ and DOC^+ that is presented here represents the first study of the relaxation dynamics of a triatomic molecular ion with the CEI technique. Both isomers were produced and investigated simultaneously, which allowed us to follow the relaxation of the bending vibrations of both isomers under identical systematic conditions and to study possible isomerization transitions of excited DOC^+ ions towards the stable DCO^+ configuration.

The paper is organized as follows: In the following section the experimental procedure is described, whereas the experimental results that could be derived directly from the data are presented in Sec. III. The calculation of the theoretical distributions and their comparison to the experimental data is given in Sec. IV, while the results are discussed in Sec. V.

II. EXPERIMENT

The Coulomb explosion imaging setup at the storage ring TSR and the analysis procedure for Coulomb explosion data have already been described in detail in a recent paper on HD^+ .²³ In the following the CEI technique is shortly summarized and the specific properties of the experiment with DCO^+ and DOC^+ ions are described.

A. Foil-induced Coulomb explosion imaging

In Coulomb explosion imaging (CEI)²² the spatial structure of a molecule is imaged by measuring the asymptotic velocities of all ionic fragments after the molecule dissociated in a Coulomb explosion process. The explosion is started by rapidly removing most of the electrons from the molecule so that the dynamics of the remaining ions is governed by the dissociative Coulomb potential. If the transition from the molecular Hamiltonian for the nuclei to the Coulomb Hamiltonian is fast compared to vibrational and rotational time scales, then the asymptotic fragment velocities yield essentially a snapshot of the spatial configuration of the molecule prior to dissociation. This is achieved in foil-induced CEI, where the molecules to be investigated are accelerated to high velocities in the laboratory frame (typically several times the Bohr velocity $V_{\text{Bohr}} = \alpha c$; α and c denote the fine structure constant and the speed of light, respectively) and are then passed through a very thin target foil (≈ 40 Å) (see Fig. 2). Due to the high velocity all binding electrons are scattered off inside the target within about 0.1 fs, while the atomic fragment ions move straight through. When they exit the foil after about 1 fs their relative positions have been modified only slightly by the Coulomb repulsion between them, which is screened by the target electron density, and by multiple small angle scattering from the target atoms. Almost all of the potential energy of the ionic fragments is then released in the Coulomb explosion in the vacuum behind the target foil. A few meters behind the target

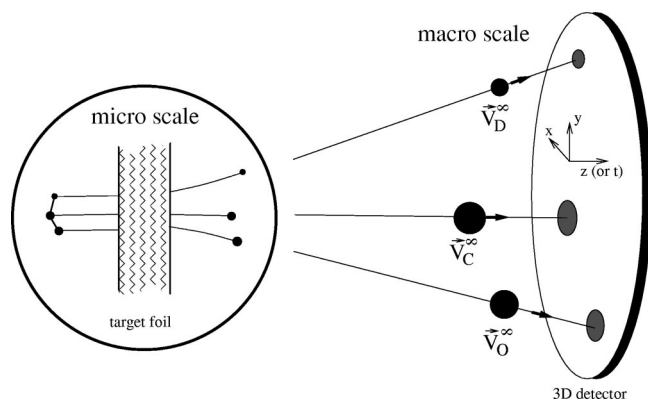


FIG. 2. Schematic picture of the Coulomb explosion imaging of a formyl molecular ion. A three-dimensional imaging detector is used to measure the three asymptotic velocity vectors ($\vec{V}_D^\infty, \vec{V}_C^\infty, \vec{V}_O^\infty$) in coincidence.

foil the asymptotic velocity vectors of all fragments are measured in coincidence using a three-dimensional multiparticle imaging detector.

The basic assumption of the CEI technique is that the potential surface that governs the dissociation dynamics is represented by a $1/R$ Coulomb potential. This is true only for fully stripped fragment ions, which can be treated as point-like charges. Fragment ions that still bind some electrons when they leave the foil only exhibit a $1/R$ potential when R is sufficiently larger than the extension of the remaining electron cloud around the ion. For fragment ions with well-bound inner-shell electrons the Coulomb potential is therefore expected to be a valid description. However, when the radius of the electron cloud is comparable to the internuclear separation this assumption does not hold anymore and a more detailed description of the explosion dynamics is required.

By measuring a set of typically 10^5 to 10^6 CEI events, probability distributions in the space of the asymptotic velocities, referred to as V space, are obtained. These V -space distributions carry the information about the distribution of

spatial configurations of the molecules prior to the explosion, referred to as R -space distribution. For a single rovibrational level, the R -space distribution is given by the square of the molecular wave function averaged over the electronic degrees of freedom. For a statistical ensemble of molecules, such as a thermal ensemble, the trace of the proper density operator is to be evaluated. Transformations from R -space distributions obtained from quantum-mechanical calculations to theoretical V -space distributions are performed by using a Monte Carlo algorithm,^{25,26} which takes into account the scattering inside the target and the detector resolutions. The Monte Carlo algorithm may also allow a numerical inversion from experimental V -space data to an experimental R -space distribution.²⁷

B. Preparation of the molecular ion beam

The DCO^+ and DOC^+ cations are produced in the fragmentation of deuterated methoxide anions CD_3O^- using the tandem van-de-Graaff accelerator of the Max-Planck-Institut für Kernphysik (see Fig. 3). A beam of methoxide anions is produced in a cesium sputter source using deuterated methanol gas and is passed into the tandem accelerator. The anions are then accelerated towards the high voltage terminal of the tandem, thereby gaining 1.67 MeV of kinetic energy, and are fragmented in collisions with a nitrogen gas stripper. All positively charged fragments are further accelerated towards the high energy exit of the tandem, where they are mass selected using a magnetic dipole field. Fragments with a mass of 30 a.m.u., expected for molecules containing one ^{12}C , one ^{16}O , and one deuterium nucleus, are separated from the other mass components and are guided to the heavy ion storage ring TSR. The total kinetic energy of the molecules amounts to 3.16 MeV, corresponding to a velocity of 2.04 a.u. ($1 \text{ a.u.} = \alpha c$).

The $\text{DCO}^+/\text{DOC}^+$ beam is then injected into the storage ring TSR (see Fig. 3), where it is stored with a $1/e$ lifetime of about 3 s, which is due to residual gas collisions despite the

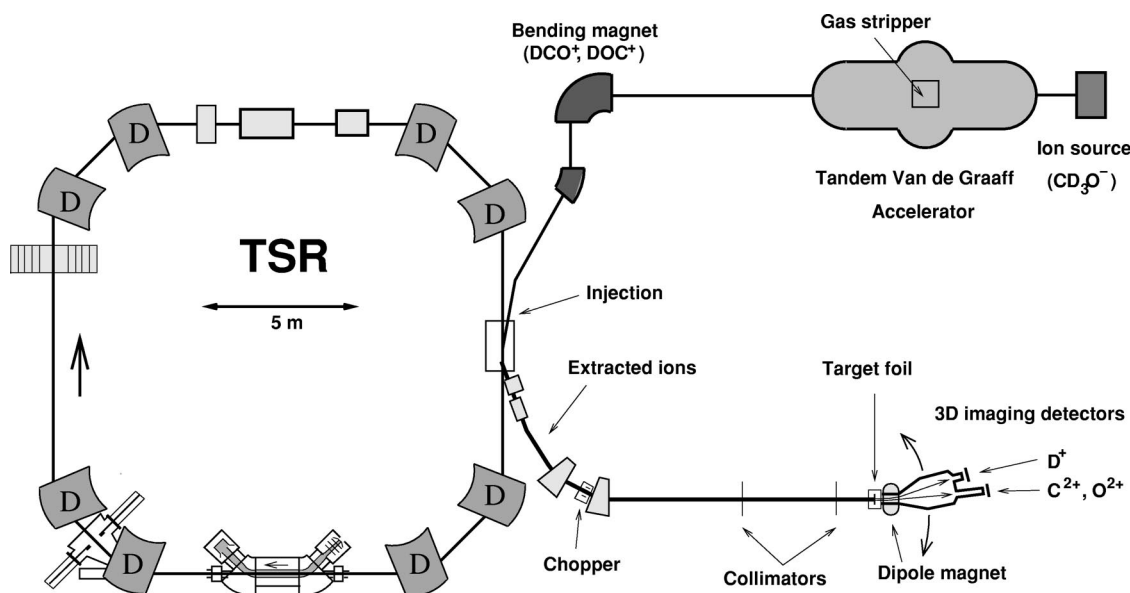


FIG. 3. Experimental setup including ion source, accelerator, storage ring TSR, and the Coulomb explosion imaging facility.

background pressure of only $5 \cdot 10^{-11}$ mbar. The storage allows rovibrationally excited molecular ions to undergo spontaneous radiative transitions, which finally lead to a molecular ion ensemble at 300 K internal temperature.²⁸ As described above, the stretching vibrations of DCO^+ and DOC^+ are expected to thermalize within several milliseconds, whereas the bending vibrational modes may take many seconds to thermalize with the 300 K background radiation field. Collisions with the residual gas result predominantly in a dissociation of the stored molecules, which is the dominant loss mechanism of the stored beam from the TSR; inelastic collisions that only transfer energy to or from the stored molecules without leading to dissociation are unlikely due to the high beam velocity. This is confirmed by our experiments on rotational and vibrational cooling of HD^{+4} and CH^+ ,²⁸ which show no sign of internal excitation due to residual gas collisions.

A small fraction of the stored molecular ions, typically 10^4 per second, is continuously extracted from the storage ring using slow beam extraction²³ and is guided to the Coulomb explosion imaging setup (see Fig. 3). Before hitting the CEI target the molecules are passed through an electrostatic chopper that is switched by the Coulomb explosion detector to allow only a single molecule at a time to be transferred to the target foil. Moreover, the molecules are collimated using two circular holes (2.5 mm in diameter, 3 m apart) before they impinge on the target foil, which consists of diamond-like carbon with an area density of $0.7 \mu\text{g}/\text{cm}^2$, corresponding to a geometrical thickness of 35 \AA .²⁹ It is mounted on a nickel mesh (transmission about 80% across a 2 mm diameter opening). The dwell time of the DCO^+ and DOC^+ ions in this target foil amounts to 0.8 fs, more than one order of magnitude faster than the time scale of the highest frequency vibration of DCO^+ . The Coulomb explosions of about 10^5 molecular ions with storage times between 2 ms and 12 s were observed and analyzed as described in the next section.

C. Measurement of the fragment velocities

The Coulomb explosion of a DCO^+ or DOC^+ molecular ion results in a deuterium, carbon, and oxygen fragment ion, the latter ones being encountered in several different charge states. The most probable charge states at the employed beam velocity range from 2+ to 4+ for carbon and 2+ to 5+ for oxygen. Using a weak dipole magnetic field downstream of the target foil (see Fig. 3), the three fragments are guided towards different positions on the two CEI detectors, depending on their charge-to-mass ratio. In this way, deuterium is well separated from the two heavy fragments. However, certain charge states of carbon and oxygen (in particular C^{3+} and O^{4+} having a charge-to-mass ratio of 1:4) are deflected to the same region of the detector, which prevents their unambiguous identification. The latter is true also for charge-to-mass ratios which do not match exactly, because each fragment hits the detector within a cone of several centimeters diameter due to the additional velocity it has acquired in the Coulomb explosion. Taking into account the accessible parameter range in terms of detector position and magnetic field, only the charge state combination of C^{2+} and O^{2+} was found to allow unambiguous identification of the

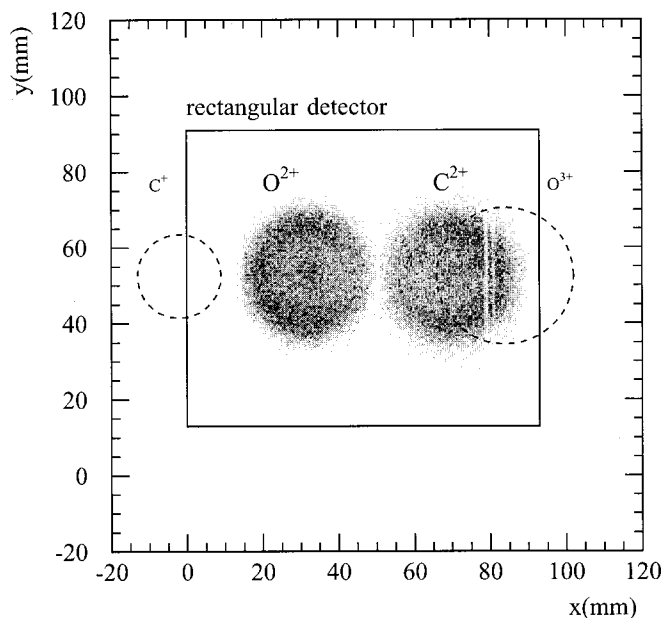


FIG. 4. Impact positions of the C^{2+} and O^{2+} fragments on one of the imaging detectors. Due to the deflection of the ions in the small magnetic field of the CEI setup, the O^{2+} ions could be unambiguously identified. The coincident fragment detected on the same detector then has to be a C^{2+} fragment. The dashed circles indicate the regions of impact for C^+ and O^{3+} ions.

particle mass. This can be seen in Fig. 4, where the measured two-dimensional distribution of the C^{2+} and O^{2+} impact positions transverse to the beam direction is plotted. The calculated impact positions of the C^+ and O^{3+} charge states are also shown. The O^{2+} fragments are observed in a region of the detector where no carbon ion can be deflected. Even though the C^{2+} charge state partly overlaps with the O^{3+} explosion cone, a C^{2+} fragment can be clearly identified if an O^{2+} fragment is detected in coincidence. Only events that are identified in this fashion as $\text{D}^+/\text{C}^{2+}/\text{O}^{2+}$ events are used in the further analysis.

The asymptotic relative velocities of the three Coulomb explosion fragments are calculated from their transverse positions and their arrival times on the two three-dimensional, multiparticle imaging detectors, which have been described in detail in Refs. 23 and 30. The deuterium fragment, which is deflected more than the heavier ions, is imaged on a circular detector of 118 mm diameter, whereas the oxygen and carbon fragments are recorded on a rectangular detector (76×93 mm) located closer to the original beam direction. Each of these detectors consists of a CsI-coated mylar foil to produce an electron shower for each fragment, a two-stage microchannel plate for amplification of the electron signal, and a phosphor screen for conversion of the electron pulse into a light spot. CCD cameras are used to measure the transverse impact positions from these light spots. The precise measurement of the relative impact times of the fragments uses timing signals that each fragment induces on thin anode strips located behind the phosphor screen. A combination of constant fraction discriminators and charge-sensitive ADC modules yields measurements of the impact times of all fragment ions relative to the first fragment hitting the detector. The achieved FWHM resolutions for impact positions and arrival times amount to about $100 \mu\text{m}$ and 200 ps, respectively. For

each event, the storage time in the TSR is also recorded.

The analysis procedure that is required to obtain the relative velocity vectors for each event from the measured data on impact positions and times has been described in detail in Ref. 31 and the general procedure can also be found in Ref. 23. After calibrating the detectors and correcting for the different deflection in the dipole magnet, the transformation of the position and time data into the nine Cartesian velocity components of the three fragments can be performed for each event. Six of these constitute the asymptotic relative velocity vectors between the fragments. Two further components describe the transverse velocities of the center of mass of the molecule and are used to check if the center of mass of the molecule did indeed remain almost unchanged during the Coulomb explosion; the part of the data ($\sim 20\%$) that is subject to center of mass deflections of more than 2 mrad away from the original beam axis is removed in the analysis. Finally, the ninth component denotes the velocity of the center of mass along the beam direction; it is derived from the revolution frequency of the molecular ions in the TSR as measured with a Schottky noise pickup.

For a triatomic molecule, three internal coordinates are sufficient to describe the relative velocities in V space. The other three relative coordinates are the angles defining the orientation of the relative velocity vectors in the laboratory space; they were used to confirm that the Coulomb explosion events occurred with random orientations of the molecular ions in the laboratory frame,³¹ similar to the findings for HD^+ .²³ For the $\text{DCO}^+/\text{DOC}^+$ system, the orthogonal Jacobi vectors of Fig. 1 are used in both R - and V -space. The three Jacobi coordinates for the internal velocities are the magnitude of the relative velocity between the carbon and the oxygen fragment, denoted V_{CO} , the magnitude of the relative velocity between the center of mass of the CO subunit and the deuterium, V_{D} , and the cosine of the angle between these two velocity vectors, $\cos \theta_V$. Typical values for the experimental FWHM resolutions amount to about $\sim 6\%$ for $\Delta V_{\text{CO}}/V_{\text{CO}}$ and $\Delta V_{\text{D}}/V_{\text{D}}$ and about absolute ~ 0.05 in $\cos \theta_V$. The Jacobi coordinate system is well adapted to the analysis of the Coulomb explosion of the two formyl isomers, because the angular coordinate $\cos \theta_V$ provides a one-dimensional coordinate in V -space that allows one to distinguish between the two isomers. Clearly, the Coulomb explosion of a linear DCO^+ ion yields a value of $\cos \theta_V = -1$, whereas for a linear DOC^+ isomer a value $\cos \theta_V = +1$ is measured. Deviations from the linear configuration in R space due to the bending vibrational motion then lead to a distribution of Jacobi angles in V space. This will be discussed further in Sec. IV. The coordinates V_{CO} and V_{D} contain information about the strength of the repulsion between the fragments, which can be related to the molecular bond lengths prior to the dissociation.

III. EXPERIMENTAL RESULTS

In the present study on isomerization and bending vibrational relaxation of DCO^+ and DOC^+ , we employ the Jacobi angle θ_V to describe the asymptotic velocities between the CEI fragments, as described in the previous section. The distributions $P(\cos \theta_V)$ of the Jacobi angle θ_V for various stor-

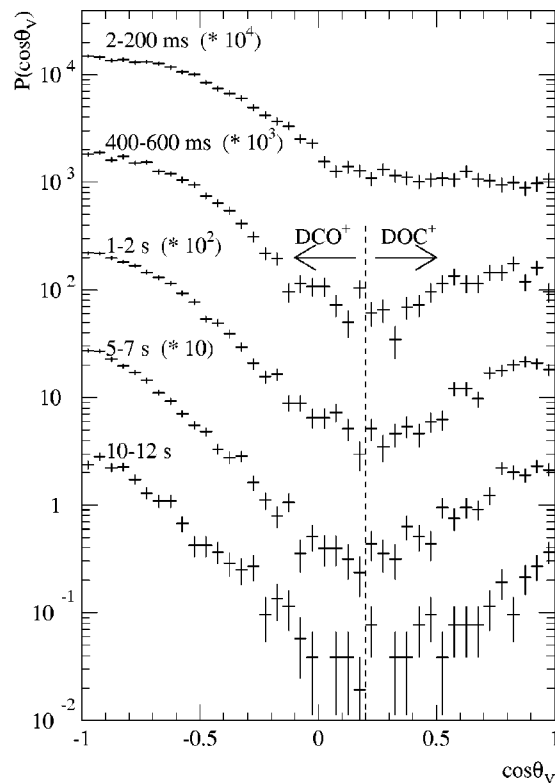


FIG. 5. Measured bending angle distribution $P(\cos \theta_V)$ of the $\text{DCO}^+/\text{DOC}^+$ ions for different storage times of the formyl ions in the TSR (the distributions are multiplied by powers of 10 for clarity).

age time intervals in the TSR are obtained by histogramming the measured values of $\cos \theta_V$. The normalized $P(\cos \theta_V)$ are shown in Fig. 5 for five different time intervals. For ease of visualization, $P(\cos \theta_V)$ in Fig. 5 are multiplied by powers of 10 and the semilogarithmic scale is used. One may note that the angular probability density $P(\cos \theta_V)$ would assume a constant value of 0.5 for an isotropic distribution.

The probability densities $P(\cos \theta_V)$ of Fig. 5 vary extensively with the storage time. For the time interval of 2–200 ms, $P(\cos \theta_V)$ shows a maximal value of 1.5 at $\cos \theta_V = -1$; it drops continuously to a value of 0.1 at $\cos \theta_V \approx 0$ and stays constant for $\cos \theta_V > 0$. After 400 to 600 ms of storage, the distribution significantly changes shape showing a minimum around $\cos \theta_V = 0.2$ with a probability density smaller than 0.1, while the probability densities near $\cos \theta_V = +1$ and $\cos \theta_V = -1$ are slightly increased. This change in the shape of $P(\cos \theta_V)$ continuously advances for longer storage times; the minimum lowers to a value of almost 0.01 for the longest time interval of 10–12 s and two clearly distinct distributions develop around $\cos \theta_V = +1$ and $\cos \theta_V = -1$ with an increasing maximum probability density and decreasing distribution width.

The two peaks observed in the probability distributions for large storage times are assigned to the two isomers of the deuterated formyl cation, with $\cos \theta_V = -1(+1)$ corresponding to the linear DCO^+ (DOC^+) configuration. Since the two distributions overlap only slightly for storage times longer than 1 s, a cut at $\cos \theta_V = 0.2$ has been used to distinguish the two isomers (see Fig. 5). This criterion has also been used for storage times less than 1 s to get at least a reasonable

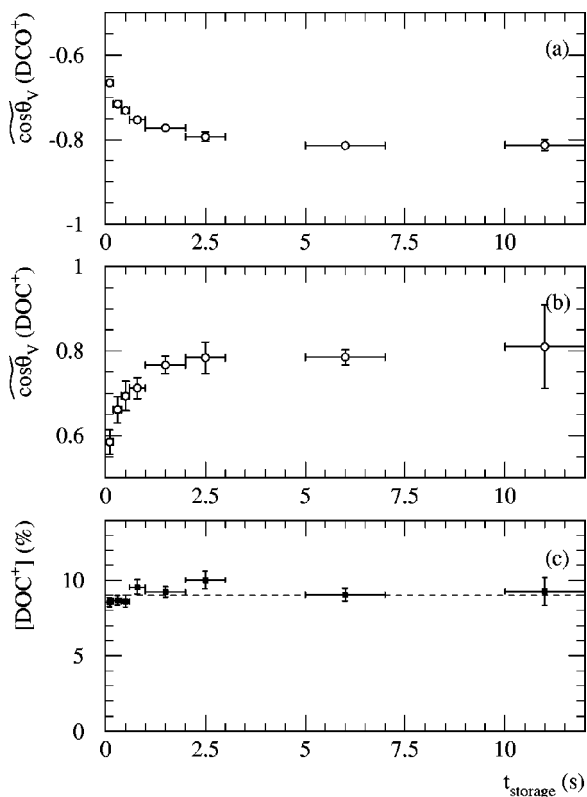


FIG. 6. Medians $\widetilde{\cos \theta_V}$ deduced with the aid of Eq. (1) from (a) the DCO^+ and (b) the DOC^+ fraction of the measured bending angle distribution $P(\cos \theta_V)$ as a function of the storage time. (c) Fraction of the DOC^+ ions in the formyl ion beam as a function of the storage time.

estimate of the isomer populations for short storage times.

In order to quantify the variation of the experimental Jacobi angle distribution with the storage time, we introduce the median $\widetilde{\cos \theta_V}$, defined by

$$\int_x^{\widetilde{\cos \theta_V}} P(\cos \theta_V) d(\cos \theta_V) = \frac{1}{2} \int_x^{0.2} P(\cos \theta_V) d(\cos \theta_V). \quad (1)$$

The latter quantity is calculated for each of the considered storage time intervals by using $x = -1$ for the DCO^+ distribution and $x = 1$ for DOC^+ . The corresponding results are displayed in Figs. 6(a) and 6(b). For DCO^+ [Fig. 6(a)], the median $\widetilde{\cos \theta_V}$ decreases with increasing time between the ion production and the Coulomb explosion measurement. The decrease to a limiting value of $\widetilde{\cos \theta_V} \sim -0.8$ occurs roughly exponentially with a time constant of approximately 900 ms. The median of the DOC^+ distribution [Fig. 6(b)] shows a similar behavior for $\widetilde{\cos \theta_V}$ values of the opposite sign since the DOC^+ distribution peaks at $\cos \theta_V = +1$ instead at -1 as for the DCO^+ distribution. The width of the DOC^+ distribution is larger than for DCO^+ and the time constant of approximately 700 ms is slightly shorter than for DCO^+ . The storage time dependence of the median seen in Figs. 6(a) and 6(b) for both isomers actually reflects the fact that the spatial structure of the molecular ions changes with storage time, which is due to the radiative relaxation of excited vibrational levels of the deuterated formyl cations during the time interval between their formation and analysis.

The fractional abundance of the metastable isomer DOC^+ in the molecular ion beam as a function of the storage time is obtained by integrating the probability density $P(\cos \theta_V)$ for $\cos \theta_V$ values larger than 0.2. We find that about 9% of the stored molecular ions belong to the DOC^+ isomer and that this fraction remains constant for storage times up to 12 s, as seen in Fig. 6(c). The error bars shown in Fig. 6(c) result from the finite statistics of the data set only; possible systematic uncertainties due to the separation cut are important only for storage times of less than 2 s and are estimated to be (on an absolute scale) 1% for 0.5 s to 2 s and about 3% for storage times of less than 0.5 s by assuming $\cos \theta_V^{\text{cut}} = 0.2 \pm 0.2$. From the constant fractional abundance of Fig. 6(c), the $1/e$ lifetime of the metastable isomer DOC^+ against isomerization into the energetically favored DCO^+ configuration is estimated to be larger than 60 s.

IV. COMPARISON TO THEORY

In this section the observed storage time dependence of the $P(\cos \theta_V)$ distributions is analyzed in terms of the vibrational excitation of the formyl ions and their radiative cooling times by comparing theoretical $P(\cos \theta_V)$ distributions to the measured data. As will be described below, the theoretical $P(\cos \theta_V)$ distributions for all relevant vibrational cation states are computed from the corresponding R -space probability distributions using a Monte Carlo model of the Coulomb explosion imaging process.

A. Probability density in R -space

Theoretical one-dimensional angular R -space probability distributions $P(\cos \theta_R)$ for DCO^+ and DOC^+ were calculated by means of the DVR-DGB method³² using a global analytical potential energy surface (PES) determined at the CCSD(T) level of theory.¹⁸ The PES employed in the present calculation was previously used to study in detail the rovibrational energy spectrum of $\text{HCO}^+/\text{HOC}^+$ and $\text{DCO}^+/\text{DOC}^+$ up to the ground state adiabatic isomerization barrier (3.6 eV above the global minimum of the PES).¹⁸ The DVR-DGB method used for the calculation of bound rovibrational levels of triatomic molecules is designed for orthogonal internal coordinates in a body-fixed reference frame and makes use of the discrete variable representation (DVR) of the angular coordinate in conjunction with a distributed Gaussian basis set (DGB) for the radial degrees of freedom.^{18,32}

Energy levels of $\text{DCO}^+/\text{DOC}^+$ are described by a set of five quantum numbers (v_1, v_2^l, v_3) and J , where v_1, v_3 are attributed to the stretching vibrations and v_2 to the bending vibration, whereas l is the vibrational angular momentum quantum number and J is the total angular momentum. For linear triatomic molecules $l = -v_2, -v_2 + 2, \dots, v_2 - 2, v_2$. One may note that vibrational levels of $l \neq 0$ are available only for $J \geq l$. Quantum number assignments to the calculated levels of $\text{DCO}^+/\text{DOC}^+$ are obtained within the DVR-DGB method in an automatic manner by means of the adiabatic projection scheme employing zero-order eigenvectors computed in the adiabatic bend approximation.¹⁸

For a rovibrational state described by (v_1, v_2^l, v_3) and J , the angular R -space distribution is calculated from the full

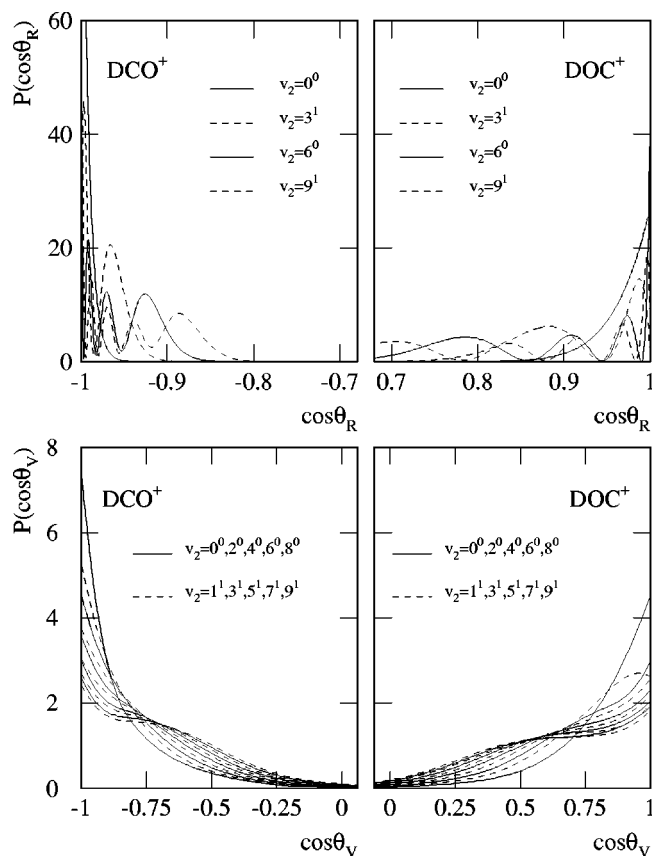


FIG. 7. Upper panels: selected R -space distributions $P_{v_2}(\cos \theta_R)$ calculated for DCO^+ and DOC^+ . Lower panels: simulated V -space densities $P_{v_2}(\cos \theta_V)$ for vibrational levels up to $v_2=9$.

dimensional nuclear wave function, $\Psi^J_{(v_1, v_2^l, v_3)}$, as the wave function amplitude squared integrated over the radial coordinates and Euler angles

$$P^J_{(v_1, v_2^l, v_3)}(\cos \theta_R) = \int_0^\infty \int_0^\infty \int_0^{2\pi} \int_0^\pi \int_0^{2\pi} |\Psi^J_{(v_1, v_2^l, v_3)}|^2 d\Omega, \quad (2)$$

where Ω stands for the two radial coordinates and three Euler angles. In the present study, only the R -space distributions $P^J_{(v_1, v_2^l, v_3)}(\cos \theta_R)$ for the first ten pure bending vibrational levels $(0, v_2^l, 0)$, with $J=l=0, 1$, are used for both deuterated formyl isomers. The vibrational levels of the excited stretching vibrations are not expected to be significantly populated on the time scale of the present experiment due to their short radiative lifetimes. The angular distributions for low-lying vibrational states are unaltered under rotational excitation, as shown by our calculations for $J=1$ and 2. In the following, the R -space distributions are therefore denoted by $P_{v_2}(\cos \theta_R)$.

The $P_{v_2}(\cos \theta_R)$ distributions for the vibrational levels of $v_2^l=0^0, 3^1, 6^0$, and 9^1 for DCO^+ and DOC^+ are shown in the upper panels of Fig. 7. Both isomers are seen to be linear molecules since $P_0(\cos \theta_R)$ of the ground vibrational level is peaked at the linear configuration ($\cos \theta_R = \pm 1$). The width of $P_{v_2}(\cos \theta_R)$ in Fig. 7 increases with the bend excitation

and is larger for DOC^+ than for DCO^+ due to the much shallower angular profile of the PES around the DOC^+ minimum (Fig. 1).

B. Coulomb explosion calculations of the V -space density

A Monte Carlo model is used to simulate the foil-induced Coulomb explosion process described in Sec. II A and to generate the theoretical V -space distributions $P_{v_2}(\cos \theta_V)$. The model is based on the Monte Carlo algorithm developed by Zajfman *et al.*^{25,26,33} for the foil-induced Coulomb explosion process and includes the effects caused by the finite experimental resolutions. The program integrates the classical equation of motion for a large sample of dissociation events. Each event initially represents a formyl ion prior to hitting the target. The initial conditions for the integration are hence obtained by Monte Carlo sampling the R -space probability distribution $P_{v_2}(\cos \theta_R)$ describing the spatial structure of the deuterated formyl cations with a specific bending vibration. The Jacobi angle θ_R defines one out of nine position coordinates. The three angles specifying the orientation of the molecule in the laboratory reference frame are chosen to yield an isotropic distribution, whereas the three coordinates of the center of mass position are set to the entrance surface of the target foil. The last two coordinates are the formyl bond lengths. These are set at their equilibrium values, since the Jacobi angle θ_V after the Coulomb explosion, being the quantity of interest in the experiment, depends only very little on the two bond lengths, i.e., the fluctuations of θ_R due to the bond length distribution is neglected. The initial velocities should also be specified for the integration of the classical motion. Apart from the overall beam velocity pointing towards the target, all velocity coordinates are set to zero. This approximation is justified by the fact that the Coulomb repulsion of the three fragments by far dominates the final velocities.

The equation of motion is integrated separately in the two regions of interest, inside the target foil and behind it. A screened Coulomb potential is used to describe the repulsion between the fragments inside the target. Scattering processes of the individual fragment atoms with target atoms are randomly introduced in the course of their motion through the target. The distance between two subsequent scattering processes is determined using a Monte Carlo method, which is based on the procedure developed by Möller, Pospiech, and Schrieder.³⁴ The scattering angle and the change of the charge state of the ion by electron stripping or capture are determined for each scattering process. When the fragments have left the foil, the interaction is changed to a Coulomb potential between point-like fragments in fixed charge states. The integration is performed until the remaining potential energy becomes smaller than a cutoff quantity ϵ , yielding the asymptotic velocity vectors of all fragments. Before the calculation of the quantity of interest, i. e., the Jacobi angle θ_V , the deflection in the magnetic field of the postdeflector and the impact positions and times on the detectors are computed and smeared by the experimental resolutions for each of the coordinates. These resolutions were determined separately

by measuring the response of the CEI detectors to alpha particles and laser pulses.³⁵ Repeating these calculations for many events, one obtains a simulated data set which can then be analyzed in exactly the same way as the experimental data to yield the theoretical V -space probability distributions $P_{v_2}(\cos \theta_V)$.

The first ten R -space distributions $P_{v_2}(\cos \theta_R)$ for both isomers have been transformed into V -space distributions using the Monte Carlo model described above. The result of this transformation is shown in the lower panels of Fig. 7. Comparison of the V -space and R -space distributions shows that the V -space distributions are much less structured than the ones in R -space, which is predominantly due to the smearing caused by multiple scattering in the target foil; the detector resolutions contribute only a minor part. Moreover, the bending angles are spread over a much larger region in V -space than in R -space. This is a consequence of the Coulomb potential and not due to any smearing, as confirmed by Monte Carlo calculations where all target effects were neglected. In fact, the magnification of a given $\cos \theta_R$ interval into a much larger interval in V -space allows one to sensitively probe molecular bond angle distributions which are subject to only small deviations from a linear configuration. For the analysis of the vibrational relaxation it is also important to note that the R -space distributions for different bending vibrational states lead to V -space distributions which differ substantially in their shape and width.

The Monte Carlo model assumes point-like ion charge distributions for the Coulomb explosion fragments. This is a good approximation when only strongly bound electrons are left with the exploding fragment ions. If this is not the case, then some electrons, while lowering the charge state of the fragment, may only partially shield the nuclear charge and the dissociation potential will therefore be steeper than expected for a pure Coulomb potential based on point charges. This effect is expected to be active in the present Coulomb explosion measurement of formyl ions, because the charge states $2+$ had to be used for the carbon and oxygen fragments in order to be able to identify them unambiguously. In fact, the effect is clearly seen in the measured V -space distributions of the relative velocities V_{CO} and V_D . These distributions are shown in Fig. 8 together with the results of Monte Carlo calculations assuming various point-like ion charge distributions. The Monte Carlo calculation based on the experimentally determined charge states $2+/2+$ is shown by a solid line. Clearly, the experimental distributions are strongly broadened towards larger relative velocities as compared to this calculation. Neither smearing effects during the 1 fs dwell time in the thin target nor a high stretching vibrational excitation of the molecule can account for these deviations. Instead, the broadening has to be attributed to deviations from a pure Coulomb potential during the first stages of the explosion in the vacuum behind the foil when the fragments are still very close to each other. Monte Carlo calculations that include this effect would require the dissociation potentials for all electronic states that lead to a fragmentation into D^+ , C^{2+} , and O^{2+} . Since these potentials are not available, limiting cases of Coulomb potentials with the screening being reduced by one or two electrons have been assumed in

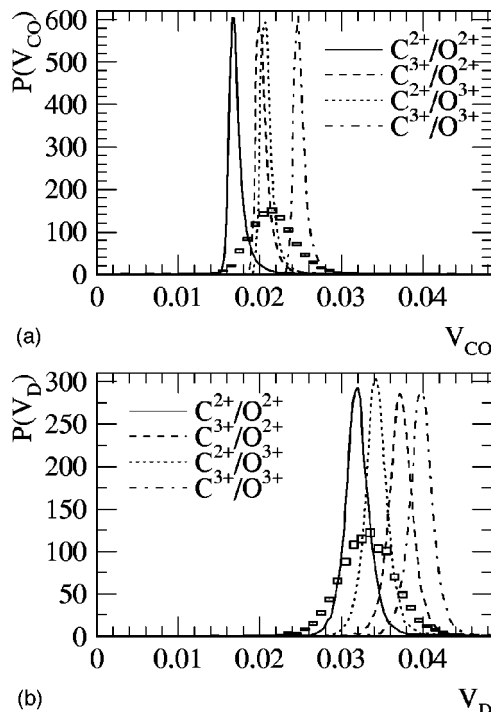


FIG. 8. Measured distributions (given by the squares) of the Jacobi velocities V_{CO} (a) and V_D (b) compared to different Coulomb explosion calculations assuming point-like charge distributions for the repelling ions after leaving the target foil.

the Monte Carlo calculations. These calculations are shown in Fig. 8 for charge state combinations $2+/3+$, $3+/2+$, and $3+/3+$ of the carbon/oxygen fragments. Obviously, the excitation of only one or two electrons into states where they screen the nuclear charge only partially is sufficient to explain the broad velocity distributions observed in the experiment.

While the velocity distributions $P(V_{CO})$ and $P(V_D)$ are strongly affected, the angular distributions $P_{v_2}(\cos \theta_V)$ are considerably less dependent on the exact shape of the dissociation potential. This is shown by performing Monte Carlo calculations of $P_{v_2}(\cos \theta_V)$ for the higher effective charge states observed to contribute to the $P(V_{CO})$ and $P(V_D)$ distributions. For low lying vibrational levels, the resulting systematic changes of the $P_{v_2}(\cos \theta_V)$ distributions turn out to be smaller than the differences in the distribution between two subsequent v_2 levels, and they increase for higher bending excitations. This is depicted in Fig. 9, where the medians $\overline{\cos \theta_V}$ of the $P_{v_2}(\cos \theta_V)$ distributions calculated with effective charge states $2+/2+$, $2+/3+$, and $3+/2+$ are shown as a function of v_2 . The $2+/3+$ charge state combination shows smaller and the $3+/2+$ combination shows larger median values than the $2+/2+$ result, while the $\overline{\cos \theta_V}$ values for the $3+/3+$ effective charge state combination (not shown) coincide with the result for $2+/2+$. Therefore, the Monte Carlo results for point-like C^{2+} and O^{2+} ions are used for comparison with the data and the deviations observed for the other charge state combinations are treated as a measure of the systematic uncertainty of the Monte Carlo calculation. Specifically, half the difference between the

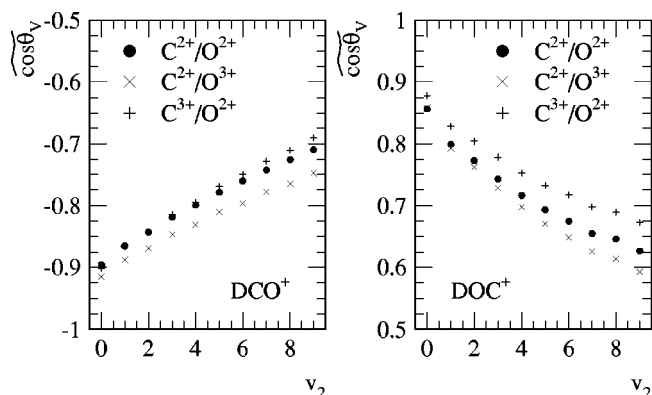


FIG. 9. Median values $\overline{\cos \theta_v}$ calculated for different bending vibrational states with quantum numbers $(0, v_2', 0)$ for DCO^+ (left panel) and DOC^+ (right panel).

$\overline{\cos \theta_v(2+/3+)}$ and $\overline{\cos \theta_v(3+/2+)}$ values was assumed as the systematic uncertainty of the most likely median values for a given bending vibrational level.

C. Bending vibrational excitation of the formyl isomers

Using the theoretical V -space results obtained in the previous section, one can now investigate the time evolution of the fundamental bending vibrational excitation of the DCO^+ and DOC^+ ions. However, the method developed to extract the time dependence of the population of individual stretching vibrational levels, already successfully applied to hydrogen ions,^{3,4,24,36} cannot be used in the analysis of the bending vibrational excitations of DCO^+ and DOC^+ as it relies on the linear independence of the theoretical V -space distributions, which is rather poorly fulfilled for the bending distributions $P_{v_2}(\cos \theta_v)$. In fact, it turns out that for $v_2 > 0$ each $P_{v_2}(\cos \theta_v)$ distribution can be approximately represented by a superposition of the distributions with $v_2 - 1$ and $v_2 + 1$, namely (see also the lower panels of Fig. 7)

$$P_{v_2}(\cos \theta_v) \approx \frac{1}{2} [P_{v_2-1}(\cos \theta_v) + P_{v_2+1}(\cos \theta_v)]. \quad (3)$$

As a consequence, the superposition

$$P(\cos \theta_v) = \sum_{v_2=0}^9 p_{v_2}(t_{\text{storage}}) P_{v_2}(\cos \theta_v), \quad (4)$$

with vibrational level populations $p_{v_2}(t_{\text{storage}})$ depends only on the mean vibrational population at t_{storage}

$$\overline{v_2} = \sum_{v_2=0}^9 p_{v_2}(t_{\text{storage}}) v_2, \quad (5)$$

and is [within the approximation of Eq. (3)] independent of all other moments of the vibrational level population. Calculations have verified that this approximation holds well for Gaussian-distributed vibrational level populations with a FWHM of up to ~ 4 vibrational levels.

The described property of the bending distributions in V space allows one to derive the mean vibrational population $\overline{v_2}$ from the measured $P(\cos \theta_v)$ distributions without using a

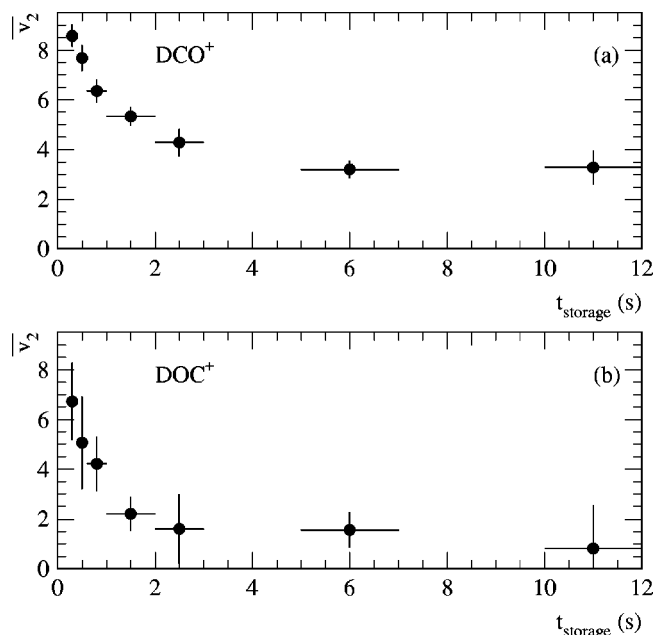


FIG. 10. Plot of the average bending vibrational quantum number $\overline{v_2}$ of (a) the DCO^+ and (b) the DOC^+ ensembles as a function of the storage time in the TSR.

complex fit to the data. Since the bending distribution $P(\cos \theta_v)$ and thus also their median value depend only on the mean vibrational population $\overline{v_2}$, the calculated dependence of the median $\overline{\cos \theta_v}$ on the individual vibrational bending vibrational quantum number v_2 shown in Fig. 9 can be reinterpreted as sampling the functional dependence of the median of $P(\cos \theta_v)$ on the mean vibrational population $\overline{v_2}$. Thus, by interpolating between the results shown in Fig. 9 one can transform the measured median values for different storage times [shown in Figs. 6(a) and 6(b)] into the mean vibrational population $\overline{v_2}$ of the stored formyl ions versus storage time. The result of this transformation is shown in Fig. 10 for both DCO^+ and DOC^+ . The error bars given include only the propagated statistical accuracies of the experimental median values. The systematic uncertainty caused by the deviations of the dissociation potential from a Coulomb law can be estimated from Fig. 9 as well. Given a fixed value of $\overline{\cos \theta_v}$, the systematic errors of $\overline{v_2}$ are about ${}_{-0}^{+1}$ for $\overline{v_2} \sim 1$, reaching values of ${}_{-1}^{+2}$ for $\overline{v_2} \sim 8$ in the case of DCO^+ and ${}_{-1}^{+3}$ at $\overline{v_2} \sim 8$ for DOC^+ . It should be noted, however, that these systematic uncertainties do not explicitly depend on the storage time and thus do not alter the general time-dependence of the observed vibrational relaxation process.

Both isomers show a fast relaxation of the bending vibration during the first 2 s of storage, with the initial vibrational population involving even higher vibrational levels than $v_2 = 9$, the highest level included in the analysis. For large storage times, the DCO^+ ions are still left with a significant vibrational excitation showing no significant sign of further relaxation; obviously, the radiative cooling time to reach the 300 K temperature of the storage ring walls, which would correspond (based on the calculated energy levels)¹⁸ to a mean vibrational population of only $\overline{v_2} \sim 0.1$, is long compared to the observation time of 12 s. For DOC^+ , there

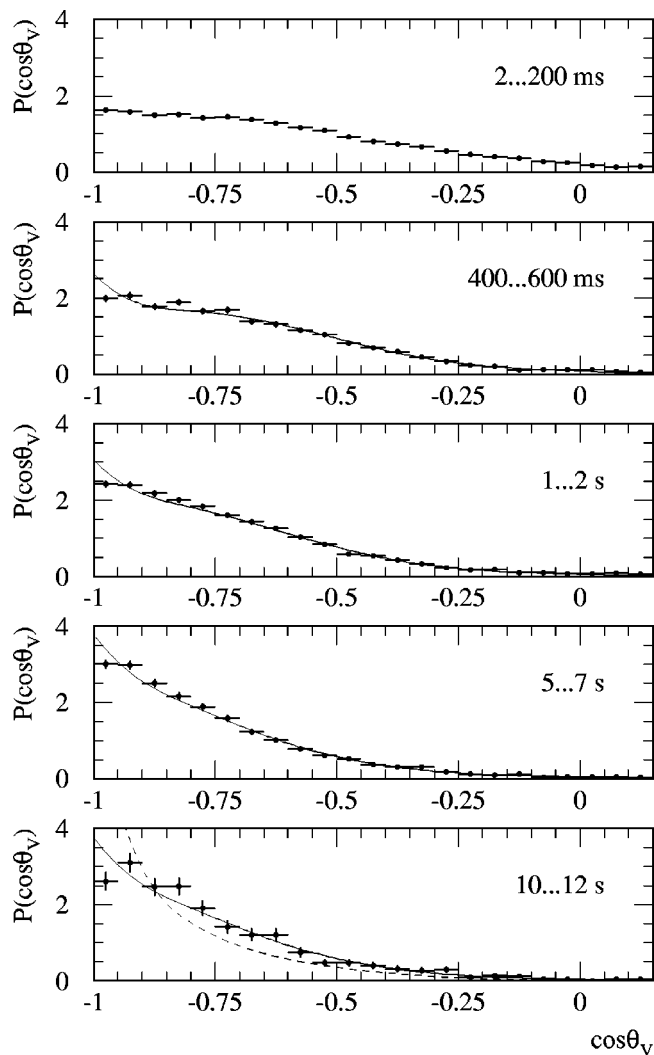


FIG. 11. Comparison of the calculated bending angle distributions (solid lines) to the DCO^+ data for different storage times. In the last bin the theoretical distribution that is expected at an equilibrium temperature of 300 K (dashed line) is also shown.

may still be some vibrational cooling taking place after the fast initial decay, but the statistics at late storage times does not allow to resolve this clearly. Moreover, for the DOC^+ ions the expected mean vibrational population for a 300 K ensemble is as high as $\bar{\nu}_2 \sim 1.4$, due to the small energy spacing,¹⁸ in agreement with the mean vibrational population observed in Fig. 10.

Employing the measured mean vibrational population values $\bar{\nu}_2$, a more detailed comparison of the experimental $P(\cos \theta_V)$ distributions to the corresponding theoretical distributions has been performed. For this purpose the vibrational population at a given storage time interval was described by a Gaussian distribution with a mean value given by the corresponding value $\bar{\nu}_2$ from Fig. 10 and a fixed variance of 0.5 vibrational levels. Note that the latter assumption is not critical because, as discussed above, the actual vibrational population distribution has very little impact on the resulting distribution $P(\cos \theta_V)$. In Figs. 11 and 12 the comparison of the measured distributions $P(\cos \theta_V)$ (crosses) with the theoretical distributions (solid line) is shown for

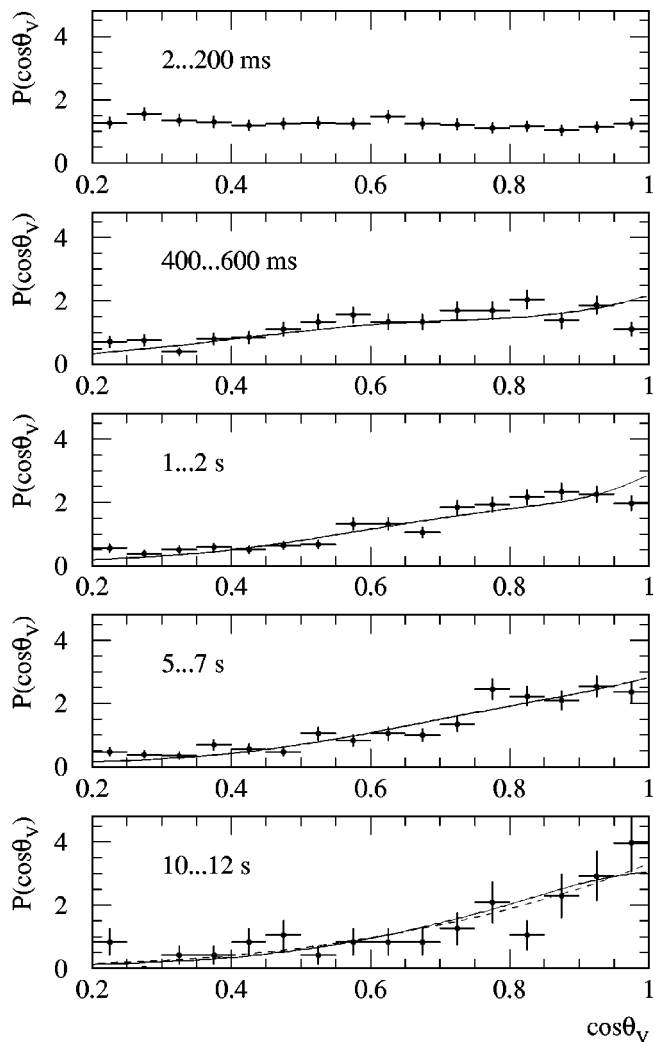


FIG. 12. Comparison of the calculated bending angle distributions (solid lines) to the DOC^+ data for different storage times. In the last bin the theoretical distribution that is expected at an equilibrium temperature of 300 K (dashed line) is also shown.

DCO^+ and DOC^+ , respectively. In the lowest panel, displaying the data for storage times between 10 and 12 s, the theoretical expectation for a thermal ensemble at 300 K is also shown as a dashed line.

The overall agreement of the shape of the theoretical and experimental distributions is reasonably good for both isomers, showing that the employed vibrational wave functions together with the Monte Carlo model describe the Coulomb explosion of the DCO^+ and DOC^+ isomers quite well. Only for the first time interval (2–200 ms) are the experimental distributions considerably broader than the theoretical curves. This originates from the fact that only vibrational levels up to $\nu_2=9$ were used in the V -space calculation, while the experimental $P(\cos \theta_V)$ distributions clearly indicate that during the first 200 ms of storage considerably higher vibrational levels are populated.

V. DISCUSSION

The experimental results indicate a constant abundance of DOC^+ molecules in the stored formyl ion beam of about

10 % for storage times between a few ms and 12 s [see Fig. 6(c)]. During this time interval the DOC^+ ions populate excited bending vibrational levels before the radiative cooling is finished. The data thus show that not only the $(0,0^0,0)$ vibrational level of DOC^+ but also the low lying excited bending vibrational levels $(0,v_2^1,0)$ do not tunnel to the DCO^+ isomer. This is in agreement with the calculation by Mladenović and Schmatz.¹⁸ They showed for the $\text{HCO}^+/\text{HOC}^+$ system that only the vibrational levels which lie less than 120 meV (for $J=0$) or 160 meV (for $J=1$) below the energy of the saddle point have a finite wave function amplitude on both sides of the potential barrier, and are therefore expected to have a finite tunneling probability. A more detailed calculation of the tunneling effects has been carried out by Gray *et al.* for the isoelectronic system HNC .³⁷ Using the reaction path Hamiltonian model, they obtained a tunneling decay constant for HNC of 10^{11} s^{-1} at an energy of about 60 meV below the classical barrier to isomerization, decreasing exponentially by about a factor of 10 for every 40 meV. They conclude that starting at about 400 meV below the classical barrier the vibrational relaxation rate can be expected to exceed the tunneling rate. Moreover, they find that the tunneling time of the vibrational ground state is much longer than the age of the universe. Nevertheless, experimental information on these tunneling times is valuable; changing the exponential dependence of the DOC^+ tunneling times on energy by a factor of 3, then tunneling times for low-lying vibrational levels would result to be of the order of seconds. Our experimental limit of $>60 \text{ s}$ for the tunneling times of the low-lying bending vibrational states of DOC^+ to DCO^+ is probing this time range.

The DOC^+ fraction of the molecular ion beam is most likely formed in a rapid isomerization from highly excited DCO^+ ions. The DCO^+ ions are produced in a collision of the precursor anion CD_3O^- with nitrogen molecules in the stripper gas target in the high voltage terminal of the tandem accelerator. At a collision energy of 1.6 MeV, this collision can be assumed to occur fast compared to vibrational time scales. The most probable DCO^+ bond angle is then given according to Franck–Condon considerations by the D–C–O bond angle in CD_3O^- , which amounts to 114° .³⁸ Since this angle deviates by only 17° from the geometry of the transition state in the $\text{DCO}^+ \rightarrow \text{DOC}^+$ isomerization process (see Fig. 1), the collision must form formyl ions with very high bending vibrational excitation—very close to or even above the barrier to isomerization. The experimental data indicate that these highly excited formyl cations isomerize with a 10% chance to the DOC^+ configuration while 90% of the ions remain on the DCO^+ side of the potential energy surface. The Franck–Condon condition assumed for the stripping collision also takes into account the high bending vibrational excitation ($v_2 > 9$) observed for both isomers at short storage times.

For the DCO^+ isomer, the relaxation of the bending vibrations with the storage time occurs mainly during the first 6 s of storage time, as depicted in the decrease of the mean vibrational population [Fig. 10(a)]. When the mean vibrational population reaches a value of about $\bar{v}_2 = 3 \pm 1$, how-

ever, further relaxation seems to be stalled within the time span investigated ($<12 \text{ s}$). A radiative lifetime of 13 s has been calculated for the $(0,1^1,0)$ vibrational level.¹⁶ Assuming that the radiative lifetimes scale like $13 \text{ s}/v_2$, as for an harmonic oscillator, a good approximation for the low lying bending levels of DCO^+ , the lifetimes of the $v_2=2$ and 3 levels are estimated to be about 6.5 and 4.3 s, respectively. The experimental data indicate that the radiative lifetimes are longer by at least a factor of 1.5, however, the statistical uncertainty of the present data does not really allow one to falsify the theoretical estimates. On the other hand, for the higher bending levels one finds that the lifetimes in the experiment seem to be at least a factor of 2 shorter than the theoretical lifetime estimates from the $13 \text{ s}/v_2$ scaling law. This may be due to anharmonic contributions to the wave functions or due to nonlinearity of the dipole moment function. Furthermore, the excited stretching vibrational levels become energetically open for bending vibrational levels with $v_2 > 3$. Possible coupling of the $(0,4^0,0)$ to the $(1,0^0,0)$ has been discussed by Hiroto *et al.*,³⁹ but Puzzarini *et al.* showed theoretically that this coupling may be weak and that the coupling of the $(1,0^0,0)$ level to the $(0,1^1,1)$ state is more important.⁴⁰ Nevertheless, coupling of the $(0,4^0,0)$ and higher bending vibrational levels to the stretching levels may be strong enough to shorten their radiative lifetimes. Clearly, accurate lifetime calculations including these effects are highly desirable.

The time dependence of the mean vibrational population \bar{v}_2 for DOC^+ [Fig. 10(b)] shows that this isomer decays radiatively within about 2–3 s to an ensemble of $\bar{v}_2 \sim 1$ that is in agreement with $\bar{v}_2 \sim 1.4$ expected for a 300 K thermal distribution. A comparison of the short time behavior of \bar{v}_2 to theoretical lifetime calculations cannot be performed, because such calculations are not available up to the present time.

VI. CONCLUSION

As a benchmark system for isomerization and bending vibrational relaxation, the internal relaxation of stored DCO^+ and DOC^+ molecular ions has been investigated on the time scale of several seconds using the technique of foil-induced Coulomb explosion imaging (CEI) combined with the heavy ion test storage ring (TSR). By measuring asymptotic fragment velocities, the CEI technique allowed us to infer information about the distribution of bond angles in the DCO^+ and DOC^+ molecules in R space. In particular, by measuring the Jacobi angle distribution $P(\cos \theta_v)$ in V -space for molecular ions prepared in the TSR with storage times between 2 ms and 12 s, the fractional abundance of the metastable DOC^+ isomer and the mean vibrational population of both DCO^+ and DOC^+ could be measured as a function of storage time. It was shown that isomerization of low-lying bending vibrational levels of DOC^+ to the DCO^+ isomer does not occur. The slow vibrational relaxation of the low bending vibrational levels in DCO^+ are found to be in qualitative agreement with theoretical lifetimes. However, more detailed calculations of the radiative lifetimes for

DCO⁺ and in particular also for DOC⁺ are desirable. It is hoped that the present experiment serves as an additional stimulus to perform these calculations.

This work has shown that the combination of the CEI technique and the storage ring TSR allows one to investigate isomerization and tunneling processes of isolated molecules on time scales that are many orders of magnitude larger than typical vibrational times. Isomerization on these time scales is very difficult to study with other experimental techniques. Future experiments are envisaged to move to larger molecules, such as HCOH⁺, which have smaller energy barriers between different structural isomers and thus can be expected to have tunneling times of no more than a few seconds, which is the accessible time scale in a storage ring experiment.

ACKNOWLEDGMENTS

The authors thank the staff of the tandem accelerator and the heavy-ion storage ring, in particular R. Repnow, R. Pfahler, V. Dürr, M. Grieser, and K. Horn, for their strong support in producing the molecular beam and carrying out the experiment. M.M. and S.S. are indebted to Professor P. Botschwina for his continuous support.

- ¹G. Mauclaire, J. Lemaire, M. Heninger, S. Fenistein, D. C. Parent, and R. Marx, *Int. J. Mass Spectrom. Ion Processes* **149/150**, 487 (1995).
- ²M. Heninger, J. Lemaire, S. Fenistein, R. Marx, and G. Mauclaire, *Int. J. Mass Spectrom. Ion Processes* **185/186/187**, 131 (1999).
- ³Z. Amitay, A. Baer, M. Dahan *et al.*, *Science* **281**, 75 (1998).
- ⁴Z. Amitay, A. Baer, M. Dahan *et al.*, *Phys. Rev. A* **60**, 3769 (1999).
- ⁵D. Buhl and L. E. Snyder, *Nature (London)* **228**, 267 (1970).
- ⁶R. Lucas and H. Liszt, *Astron. Astrophys.* **337**, 246 (1998).
- ⁷K. Kawaguchi, A. R. McKellar, and E. Hirota, *J. Chem. Phys.* **84**, 1146 (1986).
- ⁸S. C. Foster and A. R. W. McKellar, *J. Chem. Phys.* **81**, 3424 (1984).
- ⁹T. Amano, *J. Chem. Phys.* **79**, 3595 (1983).
- ¹⁰C. S. Gudeman, M. H. Begeman, J. Pfaff, and R. J. Saykally, *Phys. Rev. Lett.* **50**, 727 (1983).
- ¹¹S. C. Foster, A. R. W. McKellar, and T. J. Sears, *J. Chem. Phys.* **81**, 578 (1984).
- ¹²P. B. Davies, P. A. Hamilton, and W. J. Rothwell, *J. Chem. Phys.* **81**, 1598 (1984).
- ¹³P. B. Davies and W. J. Rothwell, *J. Chem. Phys.* **81**, 5239 (1984).
- ¹⁴K. Kawaguchi, C. Yamada, S. Saito, and E. Hirota, *J. Chem. Phys.* **82**, 1750 (1985).
- ¹⁵R. J. Foltynowicz, J. D. Robinson, and E. R. Grant, *J. Chem. Phys.* **115**, 878 (2001).
- ¹⁶P. Sebald, Ph.D. thesis, Universität Kaiserslautern, 1990.
- ¹⁷M. Bogey, C. Demuynck, and J. L. Destombes, *J. Mol. Spectrosc.* **115**, 229 (1986).
- ¹⁸M. Mladenović and S. Schmatz, *J. Chem. Phys.* **109**, 4456 (1998).
- ¹⁹T. Nakanaga and T. Amano, *J. Mol. Spectrosc.* **121**, 502 (1987).
- ²⁰R. C. Woods, C. S. Gudeman, R. L. Dickman, P. F. Goldsmith, G. R. Huguenin, W. M. Irvine, Å. Hjalmoeson, L.-Å. Nyman, and H. Olofson, *Astrophys. J.* **270**, 583 (1983).
- ²¹L. M. Ziurys and A. J. Apponi, *Astrophys. J. Lett.* **455**, L73 (1995).
- ²²Z. Vager, R. Naaman, and E. P. Kanter, *Science* **244**, 426 (1989).
- ²³R. Wester, F. Albrecht, M. Grieser *et al.*, *Nucl. Instrum. Methods Phys. Res. A* **413**, 379 (1998).
- ²⁴S. Krohn, Z. Amitay, A. Baer, D. Zajfman, M. Lange, L. Knoll, J. Levin, D. Schwalm, R. Wester, and A. Wolf, *Phys. Rev. A* **62**, 032713 (2000).
- ²⁵D. Zajfman, G. Both, E. P. Kanter, and Z. Vager, *Phys. Rev. A* **41**, 2482 (1990).
- ²⁶D. Zajfman, T. Graber, E. P. Kanter, and Z. Vager, *Phys. Rev. A* **46**, 194 (1992).
- ²⁷J. Levin, D. Kella, and Z. Vager, *Phys. Rev. A* **53**, 1469 (1996).
- ²⁸U. Hechtfischer, Z. Amitay, P. Forck, M. Lange, J. Linkemann, M. Schmitt, D. Schwalm, R. Wester, D. Zajfman, and A. Wolf, *Phys. Rev. Lett.* **80**, 2809 (1998).
- ²⁹J. Levin, L. Knoll, M. Scheffel, D. Schwalm, R. Wester, A. Wolf, A. Baer, Z. Vager, D. Zajfman, and V. Kh. Liechtenstein, *Nucl. Instrum. Methods Phys. Res. B* **168**, 268 (2000).
- ³⁰D. Kella, M. Algranati, H. Feldman *et al.*, *Nucl. Instrum. Methods Phys. Res. A* **329**, 440 (1993).
- ³¹R. Wester, Ph.D. thesis, Universität Heidelberg, 1999.
- ³²M. Mladenović and Z. Bačić, *J. Chem. Phys.* **93**, 3039 (1990).
- ³³D. Zajfman, E. P. Kanter, T. Graber, Z. Vager, and R. Naaman, *Nucl. Instrum. Methods Phys. Res. B* **67**, 22 (1992).
- ³⁴W. Möller, G. Pospiech, and G. Schrieder, *Nucl. Instrum. Methods* **130**, 265 (1975).
- ³⁵M. Scheffel, Master's thesis, Universität Heidelberg, 1999.
- ³⁶H. Kreckel, L. Knoll, S. Krohn *et al.* (unpublished).
- ³⁷S. K. Gray, W. H. Miller, Y. Yamaguchi, and H. F. Schaefer, III, *J. Chem. Phys.* **73**, 2733 (1980).
- ³⁸D. R. Yarkony, H. F. Schaefer, III, and S. Rothenberg, *J. Am. Chem. Soc.* **96**, 656 (1974).
- ³⁹E. Hirota and Y. Endo, *J. Mol. Spectrosc.* **127**, 527 (1988).
- ⁴⁰C. Puzzarini, R. Tarroni, P. Palmieri, S. Carter, and L. Dore, *Mol. Phys.* **87**, 879 (1996).